INTERNATIONAL JOURNAL FOR NUMERICAL METHODS IN FLUIDS
Int. J. Numer. Meth. Fluids 2003; **41**:303–317 (DOI: 10.1002/fld.438)

The prediction of spatially periodic flows using a finite-volume model

Tamer El Soukkary[‡] and Anthony G. Straatman[*,†,§]

The Advanced Fluid Mechanics Research Group, Department of Mechanical & Materials Engineering, The University of Western Ontario, London, Ont., Canada N6A 5B9

SUMMARY

A periodic boundary condition has been developed that can be used in conjunction with a specified flow rate to produce accurate results in spatially periodic geometries. This condition is useful in situations where the flow rate is known, or more importantly, in cases where the pressure gradient is not known *a priori*, such as in countercurrent flows. Using the present condition, the flow rate is imposed at the inlet in terms of a bulk velocity, but the velocity field evolves as part of the solution. The condition is formulated to be suitable for both fixed and moving periodic domains. For the case of a moving domain, a correction is introduced to account for changes in the instantaneous velocity through the periodic edges. Under periodic conditions, these corrections integrate to zero over a complete (temporal) period. The new periodic condition is shown to produce accurate results for flat and wavy-walled channels under both induced flow and countercurrent conditions. Copyright © 2003 John Wiley & Sons, Ltd.

KEY WORDS: finite-volume method; spatially periodic flows; periodic boundary condition

1. INTRODUCTION

In computational fluid dynamics (CFD), it is often necessary to reduce the physical extent of a computational domain to make problems practical to solve. While this process relies somewhat on the creativity of the user, it is more often reliant on the capability of the CFD code in terms of boundary conditions. In many practical situations, it is possible to reduce the physical domain into a representative spatially periodic section. Examples of such flows include tube bundles in heat exchangers, blade passages in turbomachines, wavy tubes and channels, and wavy surface driven flows. In these cases, either open or periodic boundary conditions must be employed on the periodic edges of the domain. The flows of central

* Correspondence to: A. G. Straatman, Advanced Fluid Mechanics Research Group, Department of Mechanical and Materials Engineering, University of Western Ontario, London, Ontario, Canada N6A 5B9.
† E-mail: astraat@engga.uwo.ca
‡ Research Assistant.
§ Associate Professor.

Contract/grant sponsor: Natural Sciences and Engineering Research Council of Canada

Received January 2002
Revised 12 August 2002

interest in the present work are surface-driven, countercurrent flows in which a shear-driven surface layer is opposed by a pressure-driven lower layer yielding a zero net mass flux. This flow serves as a model to describe the flow in closed basins of water driven by wind. Depending on the surface conditions, a countercurrent flow results that is driven by either a smooth or wavy upper surface.

The use of periodic boundary conditions is not new. In fact, all commercially available CFD codes have some form of periodic, open or combined condition for domain boundaries. While there is no standard method for implementing these conditions, Sani and Gresho [1] suggest the qualities that such conditions should possess: *they should permit both the flow and anything it carries to exit the domain gracefully and passively and not have any effect on the behaviour of the solution in the domain near the open boundary* (*and especially far from it*); *they should be transparent*; *they should lead to the same solution inside the common domain no matter where truncation occurred.* These qualities are accompanied by a series of mathematical constraints that are felt to ensure satisfaction of the above characteristics. While such qualities are desirable, it is not always practical to expect all such conditions to be perfectly satisfied. Progress in the development of periodic or open boundary conditions must also be measured in terms of extensions that lead to increased modelling capability and elucidation on physics. All extensions can be considered useful provided the user is aware of the approximations inherent in the conditions used.

Recently, Nicolas *et al.* [2] compared five different types of open and periodic boundary conditions in the computation of Poiseuille–Bénard channel flow. This is essentially a mixed-convection flow in a horizontal channel heated from below. For the two-dimensional case, the flow consists of a series of contra-rotative rolls *flowing* through the domain. The results showed good flow behaviour when Orlanski-type [3] open boundary conditions were used, but other types of open conditions were found to be unstable. They also found that the use of periodic boundary conditions gave excellent results and allowed for further reductions in the size of the computational domain over that required for convergence of the same problem using open conditions. The condition used required the imposition of a constant pressure gradient to induce a flow through the domain. While this type of condition is suitable for many situations, in cases where the flow rate is known, such as in a wavy tube or channel, it would be more convenient to impose the mass flow directly at the periodic boundary and allow the pressure field to evolve as part of the solution. Furthermore, in countercurrent flows, the pressure gradient is not known *a priori* so a periodic condition that imposes the mass flow rate is necessary. It is noted that some commercial CFD packages do allow the user to specify either a periodic pressure drop or a mass flux in combination with a periodic boundary condition. However, numerically both conditions are handled using some variant of the pressure-gradient approach described above. That is, if a mass flux is specified, a pressure drop is *guessed* and then systematically varied until the mass flux reaches the desired value to within some numerical tolerance.

In the present study, a unique periodic condition is developed for use in modelling spatially periodic flows. As discussed above, the flows of central interest are spatially periodic, countercurrent flows such as those observed in closed surface-driven bodies of water. The periodic condition includes the imposition of a net mass flow (which is zero for counter-current flows) through the periodic boundaries. Further, the condition is formulated to accommodate wavy-driven-surfaces for which the size of the periodic boundaries change with time. This periodic condition is useful not only in countercurrent flows, but also in flows where it is desirable

to specify the mass flux across a periodic boundary without fixing the velocity profile. A unique implementation for the developed condition is presented that is shown to be extremely useful for the prediction of several types of spatially periodic flows in which the flow is either pressure driven or surface induced. The boundary conditions are implemented into a finite-volume algorithm that utilizes an adaptive, moving grid formulation. Subsequent sections of the paper describe the governing equations and numerical formulation, the development and implementation of the boundary conditions, and validation of the periodic condition by computing the flow through smooth and wavy channels and fully developed countercurrent flow with a smooth or wavy upper surface.

2. GOVERNING EQUATIONS AND NUMERICAL FORMULATION

Predictions of incompressible, Newtonian, laminar flow are obtained by solving the conservation of mass and momentum equations in the form

$$\frac{\partial \rho}{\partial t} + (\rho U_i)_{,i} = 0 \tag{1}$$

and

$$\frac{\partial}{\partial t}(\rho U_i) + (\rho U_k U_i)_{,k} = -P_{,i} + \mu(U_{i,k})_{,k} \tag{2}$$

where U_i is the fluid velocity in the x_i direction, P is the pressure, and ρ and μ are the fluid density and dynamic viscosity, respectively.

The transport equations are solved numerically using the structured finite-volume approach described by Patankar [4], except with a collocated variable arrangement. (Extensions for the adaptive grid formulation are described in Reference [5] and are not repeated here.) Application of this procedure results in a series of discrete algebraic equations that take the form

$$a_P^{\phi}\phi_P = \sum a_{\mathrm{nb}}^{\phi}\phi_{\mathrm{nb}} + b_P^{\phi} \tag{3}$$

in which the a^{ϕ} terms are the active coefficients on ϕ, ϕ represents any dependent variable, and nb implies summation over the neighbouring nodes. For the method adopted in this work, only neighbouring nodes that share a face with the volume under consideration are included implicitly in the numerical formulation. As such, the neighbouring nodes are those to the west, W; east, E; south, S; and north, N; of P for two-dimensional computations. Figure 1 illustrates the grid configuration and shows the indices used to describe the extent of the domain. Using this configuration, (ib, jb) denotes the first interior control volume and (ie, je) denotes the last interior control volume. Boundary conditions are required over the $jb-1, je+1, ib-1$ and $ie+1$ edges of the domain.

The mass and momentum equations are solved as a coupled set and thus, no semi-implicit technique (e.g. SIMPLE) is required to maintain the coupling between the mass and momentum equations. Thus, for the mass and momentum set, Equation (3) is recast as

$$\mathscr{A}_P\{\phi\}_P = \sum \mathscr{A}_{\mathrm{nb}}\{\phi\}_{\mathrm{nb}} + \mathscr{B}_P \tag{4}$$

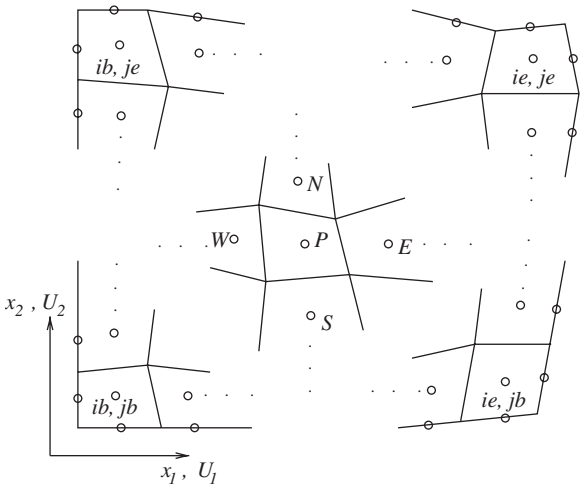

Figure 1. Configuration of a typical grid showing the co-ordinate system and the grid indices.

where the $\mathscr{A}$ terms are now 3×3 matrices of active coefficients, $\{\phi\}$ is a 3×1 vector of components P, U_1 and U_2, and $\mathscr{B}_P$ is a 3×1 vector of source terms. Despite the direct, implicit coupling between the mass and momentum equations, there still exists the possibility of checker-board solutions of pressure and velocity being accepted as smooth. To remove this possibility, the fourth-order pressure smoothing technique originally proposed by Rhie and Chow [6] has been implemented.

Convective fluxes in the transport equations were discretized using the central difference scheme (CDS). This scheme is second-order accurate and was implemented using the deferred correction approach described in Reference [5], whereby the convection through the east face, for example, is written as

$$F_e = F_e^{\mathrm{UDS}} + (F_e^{\mathrm{HOS}} - F_e^{\mathrm{UDS}})^{m-1} \tag{5}$$

In Equation (5), F_e^{UDS} is the convective flux evaluated using the first-order upstream differencing scheme (UDS) and F_e^{HOS} is the flux evaluated using the higher-order scheme. Using this approach, the UDS flux is treated implicitly and the terms in parenthesis are evaluated from the previous iteration and summed into the source terms as a deferred correction. In this manner, there exists no possibility for the active coefficients to become negative in the iterative procedure and the converged solution is second-order accurate. The discrete equations were solved using the semi-implicit block solver WATsitB [7]. The coupled mass-momentum set was formed into blocks and solved simultaneously.

3. THE PERIODIC BOUNDARY CONDITION

Consider the two different domains shown in Figure 2. If the left and right edges of domains (a) and (b) are open at $\pm\infty$ and the upper and lower surfaces are fixed, then with fluid

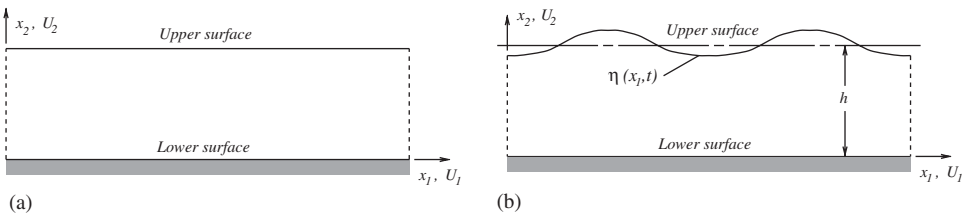

Figure 2. Schematics of the two geometries considered in the present work. Geometry (a) represents a plane channel when both surfaces are fixed and smooth countercurrent flow when the upper surface is moving. Geometry (b) represents a wavy channel when both surfaces are fixed and wavy countercurrent flow when the upper surface is moving.

motion in the x_1 direction, domain (a) would produce plane channel flow and domain (b) would produce spatially periodic, channel flow. If the left and right edges are closed at $\pm\infty$ and the upper surface is in motion while the lower surface is fixed, then domain (a) would produce fully developed countercurrent flow and domain (b) would produce spatially periodic countercurrent flow. Note that in domain (b), the flow is quite different if the lower surface moves while fixing the upper surface. In all cases, the flow produced is spatially periodic in nature (for the flat upper surface, the flows are more often described as fully developed). To compute these flows, no-slip/zero-penetration conditions are imposed on the upper and lower surfaces and the pressure on these surfaces is extrapolated from within the domain. In both domains, and for all flows considered, the periodic boundaries are the left and right edges of the domain.

The configuration required for the periodic boundary condition developed herein is similar to that described in Nicolas *et al.* [2], i.e. the periodic domain is reduced to two complete periods, as shown in Figure 2(b). For the case of flat upper and lower surfaces, the length of the domain is inconsequential, but, a certain minimum number of volumes must be used to accommodate the periodic conditions, as will be made evident below. In Nicolas' implementation of the periodic boundary condition, the flow was induced through the channel by imposing a constant pressure gradient between the inlet and exit boundaries of the channel. While this condition is suitable in channel flow, it is not appropriate for countercurrent flows where the structure is established by a shear-driven layer opposing a pressure-driven layer. In the present work, the flow rate is imposed across the inlet boundary in terms of velocity, and the pressure level is specified across the outlet boundary. The velocity and pressure fields are allowed to develop as part of the solution. The shape of the inlet velocity profile is obtained from the outlet boundary and the shape of the pressure profile is obtained from the middle section of the domain. Figure 3 shows the transfer of information used in the imposition of the periodic boundary condition. The exact implementation of the boundary conditions and the transfer of information are described below.

At the outlet of the domain, the condition on the U_1 velocity component is obtained from the conservation of mass equation. The U_1 velocity can be solved discretely to give

$$(U_1)_{ie+1,j} = (U_1)_{ie,j} - \Delta x_1 \left.\frac{\mathrm{d}U_2}{\mathrm{d}x_2}\right|_{ie,j} \tag{6}$$

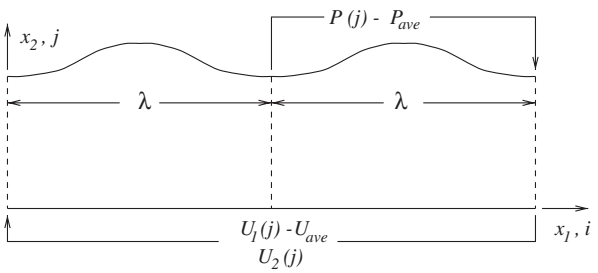

Figure 3. Schematic showing the imposition of the periodic boundary condition and the transfer of information.

When the gradient term vanishes, as in fully developed flows, the condition relaxes to the commonly used zero-gradient condition. While the zero-gradient condition is typically more robust, the correction from the mass equation allows for flow development at the domain outlet and is thus, more accurate in cases where the domain is irregular and the flow is not fully developed. In terms of the active coefficients on the boundary nodes, the outlet boundary condition on U_1 is implemented as

$$a_P(ie+1,j) = 1.0$$

$$a_{\mathrm{W}}(ie+1,j) = 1.0$$

$$a_{\mathrm{E}}(ie+1,j) = 0.0$$

$$a_{\mathrm{S}}(ie+1,j) = 0.0$$

$$a_{\mathrm{N}}(ie+1,j) = 0.0$$

$$b(ie+1,j) = -\Delta x_1 (\mathrm{d}U_2/\mathrm{d}x_2)|_{ie,j}$$

where Δx_1 is the horizontal distance between nodes (ie,j) and $(ie+1,j)$, and $-(\mathrm{d}U_2/\mathrm{d}x_2)|_{ie,j}$ is obtained by integration over the faces of the volume centred at (ie,j) (as described in Reference [5]).

For the U_2 velocity at the outlet, information is transferred from the middle section of the domain. In this manner, the velocity field at the outlet is not restricted in any way. For cases where the velocity gradients are small, it may also be suitable to employ a zero-gradient condition, which leads to $U_2(ie+1,j) \approx U_2(ie,j)$ across the outlet. The outlet condition on U_2 is implemented similar to that described above for U_1.

Information on U_1 and U_2 from the outlet boundary are then transferred face by face to the inlet and corrected to maintain the desired mass flow rate. The correction on the U_1 velocity is obtained by computing the integrated flow rate across the outlet

$$\dot{Q} = \sum_{j=jb}^{je} (U_1)_{ie+1,j} C^e_{ie,j} \tag{7}$$

and then the bulk velocity

$$U_b = \frac{\dot{Q}}{\sum_{j=jb}^{je} C^e_{ie,j}} \tag{8}$$

where $C^e_{ie,j}$ is the area of the east face of the control-volume centred at (ie, j). At the inlet, this condition is implemented discretely into the U_1 equation as

$$a_P(ib-1,j) = 1.0$$
$$a_{\mathrm{W}}(ib-1,j) = 0.0$$
$$a_{\mathrm{E}}(ib-1,j) = 0.0$$
$$a_{\mathrm{S}}(ib-1,j) = 0.0$$
$$a_{\mathrm{N}}(ib-1,j) = 0.0$$
$$b(ib-1,j) = U_1(ie+1,j) + (U_{\mathrm{desired}} - U_b)$$

Because of the conservative nature of the finite-volume method, the bulk velocity is always close to U_{desired} and thus, the correction is always small. The correction is essentially a mechanism to avoid having the imposed velocity change as a result of accumulated numerical errors. Again, the implementation for the U_2 velocity is similar except that no correction for flow is necessary. As such, the U_2 velocity is simply transferred from the outlet to the inlet. Upon convergence, the inlet and outlet profiles for both U_1 and U_2 are identical, to satisfy the periodic condition. As will be seen, this implementation is extremely robust and results in accurate solutions for all of the flows considered in this study. It is also noted that the present condition is not sensitive to the positioning of the periodic boundaries, i.e. the boundaries can be placed in regions of developing and recirculating flow without loss of accuracy, as will be seen in the forthcoming validations.

The implementation for the condition on pressure is similar to that described above. Information is transferred from the center section of the domain to obtain the shape of the pressure profile. The average pressure is obtained as

$$P_{\mathrm{ave}} = \frac{\sum_{j=jb}^{je} 0.5(P_{ic,j} + P_{ic+1,j}) C^e_{ic,j}}{\sum_{j=jb}^{je} C^e_{ic,j}} \tag{9}$$

where P_{ave} is the average pressure required to apply the same force over the centre section of the domain and ic is the i index of the volumes adjacent to (and left of) the centreline of the domain. As indicated, the pressure is first interpolated to the face and then multiplied by the area to obtain the component force. The pressure profile is then transferred to the outlet of the domain and corrected to yield the desired average pressure across the outlet. Discretely, this is implemented as

$$a_P(ie+1,j) = 1.0$$
$$a_{\mathrm{W}}(ie+1,j) = 0.0$$

$$a_{\mathrm{E}}(ie+1,j)=0.0$$
$$a_{\mathrm{S}}(ie+1,j)=0.0$$
$$a_{\mathrm{N}}(ie+1,j)=0.0$$
$$b(ie+1,j)=0.5*(P(ic,j)+P(ic+1,j))+(P_{\mathrm{desired}}-P_{\mathrm{ave}})$$

At the inlet of the domain, the pressure is simply extrapolated, as is done for the solid walls. Upon convergence, the x_2 variation of pressure is virtually identical at the inlet, the centre and the outlet, but they are shifted to yield the appropriate overall pressure gradient required to drive the desired mass flow.

The conditions described above are suitable for all cases where the domain boundaries are fixed, or in motion but flat. For the case of a wavy, moving surface, the size of the inlet and outlet boundaries changes with time so, in general, the applied conditions must also change. Note however, that at all instants in time the inlet and outlet remain exactly periodic. Figure 2(b) shows a wavy-walled channel for which the upper surface is described by

$$\eta(x_1,t)=A\cos[k(x_1-ct)] \tag{10}$$

where $\eta(x_1,t)$ oscillates about the mean depth level h. In Equation (10), A is the amplitude about the mean depth level, $k=2\pi/\lambda$ is the wave number, λ is the wavelength, c is the wave speed and t is time. In simulating this case, the upper and lower surfaces are modelled as smooth walls and thus no-slip, zero-penetration conditions must be imposed on the velocity components. Since the upper surface moves at c, following Equation (10), the horizontal velocity on this surface takes the value $U_1=c$. If the upper surface is considered solid, the U_2 velocity can be devised intuitively as $U_2=0$. The same result arises if the upper surface is considered to be a free-surface wave travelling at c with a particle drift velocity $U_1=c$. For this case, the kinematic condition is

$$U_2=\frac{\partial\eta}{\partial t}+\frac{\partial\eta}{\partial x_1}U_1$$

which also yields $U_2=0$.

The periodic conditions on the left and right edges of the domain are implemented as described above, except with a correction on the horizontal velocity to account for the temporal variation of the edges. The fact that a correction is necessary is easily seen in Figure 4, which shows one spatial period of the domain at an arbitrary instant in time. The dashed line in part (a) of the figure represents a control-volume over which a mass balance can be taken. Figure 4(b) shows the stated control-volume with all of the mass fluxes to be considered. Assuming a unit depth, the mass fluxes over the faces of the control-volume can be computed. Since the left boundary of the control-volume passes through the mean depth level, $\dot{m}_1=0$. The mass flux through the lower boundary is also $\dot{m}_4=0$. The mass flux through the upper boundary for any instant in time can be obtained as

$$\dot{m}_3=\sum_i(\rho c)C^n_{i,je}n_x \tag{11}$$

where $C^n_{i,je}$ is the area of the north face of a cell centred at (i,je) and n_x is the horizontal component of the unit normal vector for the C_n face. Since $c=U_{\mathrm{s}}$, summation over the

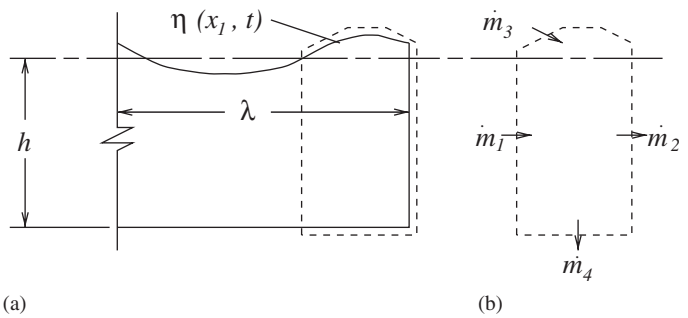

Figure 4. Schematic showing the mass flux correction required in cases where the physical boundary changes as a function of time.

upper face yields

$$\dot{m}_3 = \rho U_s \eta(x_{1,o}, t) \tag{12}$$

where $\eta(x_{1,o}, t)$ is the surface position with respect to the mean depth level at the domain outlet. The mass flux through the outlet boundary, $\dot{m}_2$, is not known and must be found from a mass balance over the control-volume, which yields

$$\dot{m}_2 = \dot{m}_3 = \rho U_s \eta(x_{1,o}, t) \tag{13}$$

Based on Equations (12) and (13), it is evident that if a complete period is considered, the mass flux through the right boundary is exactly zero. It is also noted that Equation (13) is valid independent of where the left edge of the control-volume is positioned because the slight non-zero mass flux through the left edge is balanced by the additional mass flux through the upper boundary. The instantaneous bulk velocity through the outlet (right edge) of the domain is then obtained from

$$U_{bm} = \frac{\dot{m}_2}{\rho \sum_{j=jb}^{je} C_{ie,j}^{e}} = U_s \frac{\eta(x_{1,o}, t)}{h + \eta(x_{1,o}, t)} \tag{14}$$

It is easily shown that U_{bm} satisfies the physical condition that the corrected mass flow must integrate to zero over one (or several) complete periods. In terms of the implementation, U_{bm} simply replaces U_b in the source term b; no additional changes are required. The solution for the case with a moving, wavy upper surface must be obtained as a transient calculation. As such, the grid is modified at the start of a time step, followed by a calculation of U_{bm}, which is then fixed for that time increment. The solution is obtained for this condition before advancing to the next time level. Validation of the periodic boundary condition is carried out in the next section for both steady and transient cases.

4. VALIDATION

To validate the periodic condition developed in the present work, computations are presented for the four cases described at the beginning of the previous section, i.e. the flat and

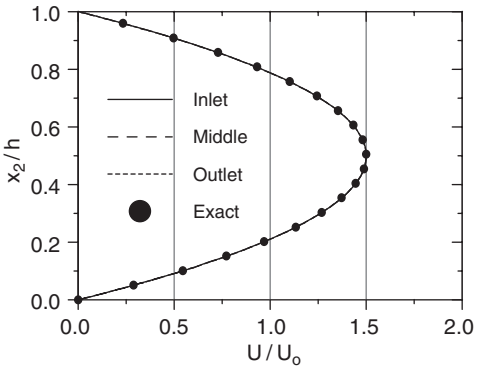

Figure 5. The horizontal velocity, U_1/U_0 plotted as a function of x_2/h at three positions for the smooth, channel flow.

wavy-walled channels and the flat and wavy surface-driven countercurrent flows. For consistency, the computational domain for all cases was nominally $2\lambda \times h$ in the x_1 and x_2 directions, respectively, where $\lambda = 0.132$ m and $h = 0.102$ m. For the wavy upper surface, the amplitude was set to $A = 0.01$ m. Computations for all cases were conducted on computational mesh sizes ranging from 60×20 to 240×80 in the x_1 and x_2 directions, respectively, to ensure that solutions were grid independent. At the highest mesh density, all solutions were spatially accurate to much better than 1% based on velocity profiles and axial pressure drops. In addition, for the driven wavy surface, a time-step independence study was conducted to ensure that the reported results were not dependent on the time-step size chosen. Using a dimensionless time-step size of $\Delta t/T = 0.066$, which corresponds to 200 steps per period, and a three-time-level discretization scheme, the temporal results were independent to better than 1%. For all cases, only laminar flow was considered.

Plane channel flow was computed for a Reynolds number $Re = U_0 h/v = 1000$, where U_0 is the mean velocity, h is the channel width and v is the fluid kinematic viscosity. While cases were computed for several other Re in the laminar regime, results are only presented here for $Re = 1000$. The left and right edges of the domain were assumed periodic with an induced flow rate $\dot{Q} = U_0 h$, and hence $U_{\text{desired}} = U_0$. The computations were initiated with $U_1 = U_0$, $U_2 = 0$ and $P = 0$ throughout the domain. The results for the U_1 velocity are shown as a function of x_2 in Figure 5 along with the exact, analytical result. The normalized solutions for three positions in the domain are shown to be coincident with each other and with the exact result, indicating the accuracy of the computed results. Pressure variations (not shown) were also predicted to be coincident with the exact solution in terms of vertical distribution and axial pressure drop, again indicating the accuracy of the solution and the conditions used.

Calculations of flow through a channel with a wavy upper wall were also performed for a Reynolds number $Re = U_0 h/v = 1000$. Boundary and initial conditions were set to be the same as those used for the plane channel with a flat upper surface. Figure 6(a) shows computed streamlines to give a qualitative picture of the flow field. It is evident from the figure that the flow is essentially channel like, except with recirculating regions that form beneath the crests of the wavy wall, as might be expected. To confirm the periodicity of the flow, results for the U_1 velocity are shown in Figure 6(b) for five positions along one period of the wavy

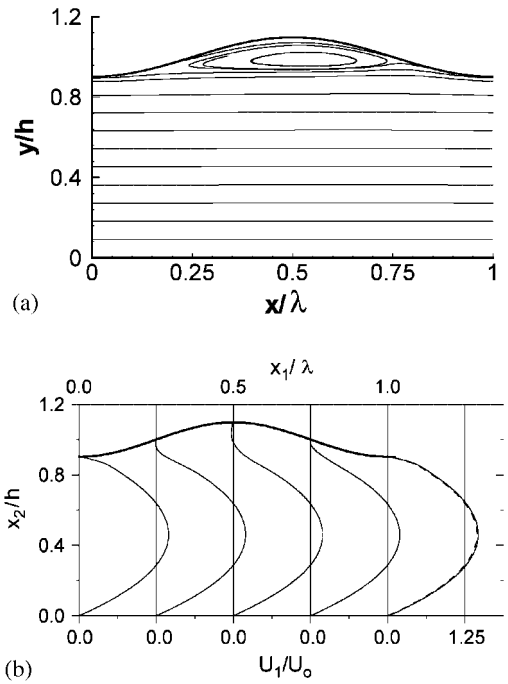

Figure 6. Streamlines (a) and U_1 velocity profiles (b) for the case of channel flow with a wavy upper surface at $Re = 1000$. In plot (b), the velocity scale is the lower abscissa and the scale showing the position of the profiles is the upper abscissa. The dashed lines represent profiles from the first periodic section while the solid lines represent the same spatial positions in the second spatially periodic section.

channel. In the figure, the solid lines represent the profiles from the first spatial period while the dashed lines represent the spatially similar profile from the second spatial period. The predicted velocities are shown to be coincident at all positions demonstrating the periodicity of the flow and the validity of the periodic condition. The velocity profiles also confirm the channel-like structure of the flow, and show the magnitude of the recirculation beneath the crests. The pressure variation along the axis of the channel is shown in Figure 7. The pressure at each axial position is the area-weighted average pressure over that section and is normalized by the dynamic pressure, $\frac{1}{2}\rho U_0^2$. The solid line represents the variation through the first periodic section and the dashed line represents the same variation in the second periodic section, shifted to coincide with that from the first section. The overall pressure drop through each section is seen to be virtually identical; however, small deviations do occur under the wave crests from section to section. The deviations do not appear to affect the velocity field and are likely a result of grid resolution. Overall, the results from the wavy-walled channel are seen to be extremely well predicted using the periodic boundary condition. A full, parametric study of wavy-walled channels conducted using a perturbation method and the boundary condition developed herein is given in Zhou *et al.* [8].

The countercurrent flow cases were computed for several Reynolds numbers, however again, in the interest of brevity, results are only reported here for $Re = U_s h/v = 1000$, where U_s is the

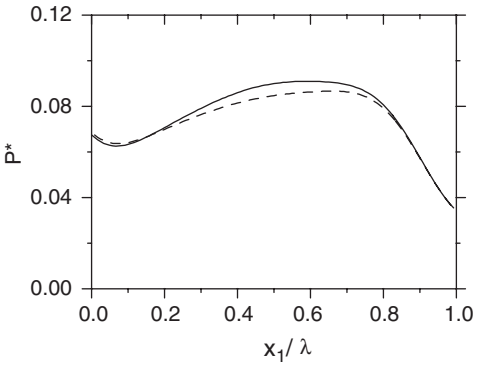

Figure 7. Plot of the dimensionless axial pressure variation for wavy channel flow.

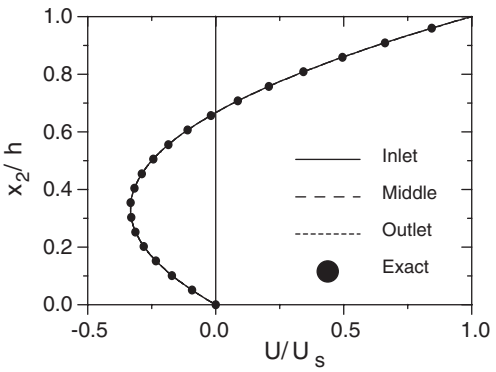

Figure 8. The horizontal velocity, U_1/U_s plotted as a function of x_2/h at three positions for countercurrent flow driven by a smooth upper surface.

surface speed. A full parametric study of countercurrent flows is considered for future work, but is beyond the scope of the present paper. Since both geometric cases represent countercurrent flow, the periodic conditions include $U_{\text{desired}} = 0$, i.e. the result is a shear-driven surface layer opposed by a pressure-driven lower layer. The computations for both geometries were initiated with $U_1 = U_2 = P = 0$, with a surface speed U_s. Results for countercurrent flow with a flat upper surface are given in Figure 8. The figure shows the predicted U_1 velocity profile as a function of x_2 for three different sections of the domain along with the analytical solution for laminar, countercurrent flow. The velocity profiles are seen to be virtually indistinguishable, indicating the accuracy of the solution and the validity of the boundary conditions used. While not shown, the axial pressure variation was computed to within 0.2% of the exact solution.

The moving, wavy-surface case was run as a transient calculation using a three-time-level method. Computations were run for 10 complete periods to remove cycle-to-cycle variations. The time-periodic results are shown in Figure 9(a)–(d). Figure 9 shows velocity profiles and streamline plots for four evenly spaced time intervals, $t/T = 0, 0.25, 0.5$ and 0.75. Clearly, the flow is fully quantified by any one plot, since the flow is stationary with respect to a reference

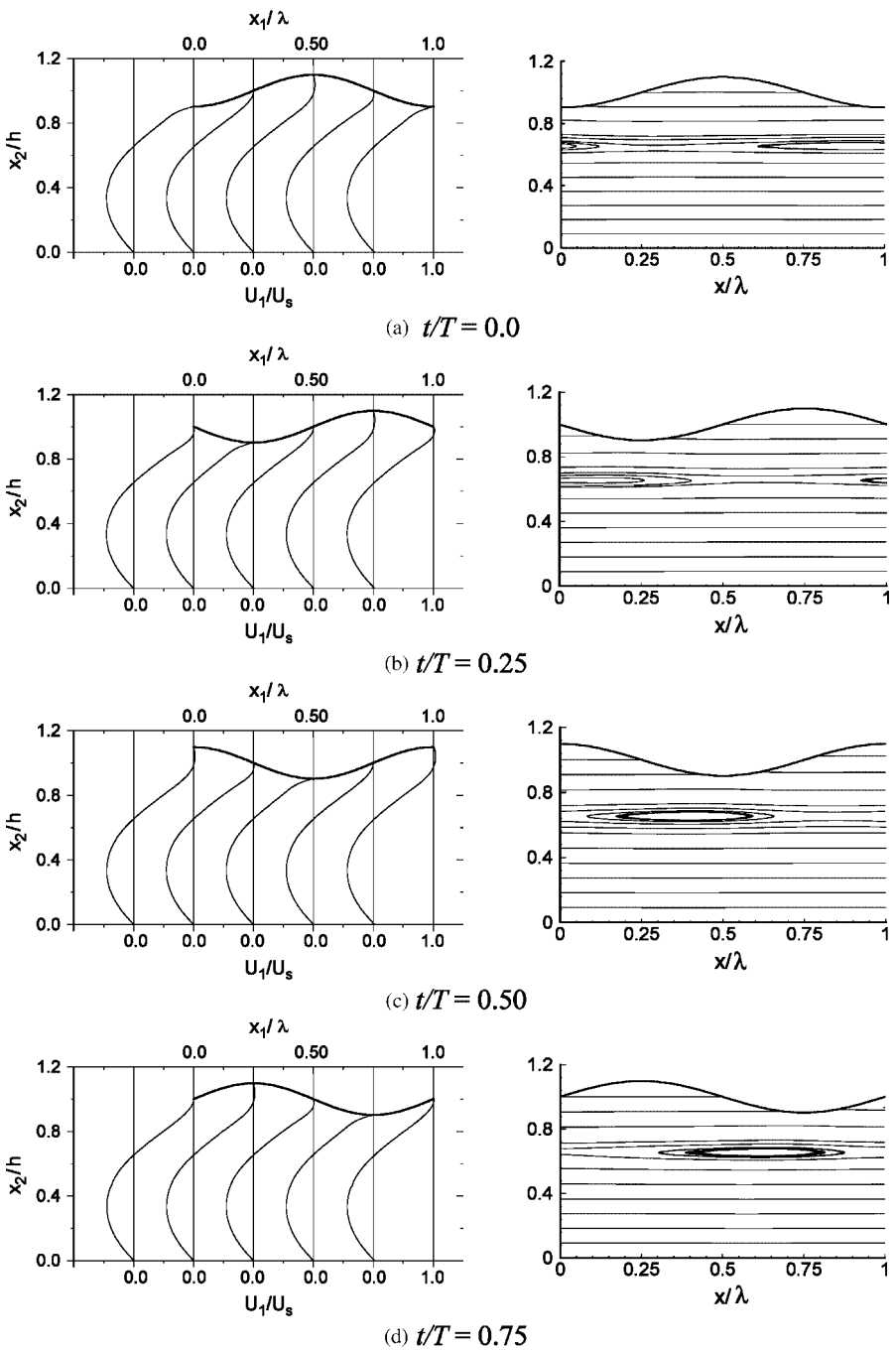

Figure 9. Velocity profiles and streamlines for countercurrent flow driven by a wavy upper surface. Results are shown for four equally spaced time intervals as indicated in (a) through (d). Velocity profiles are shown for five positions along one period of the wavy domain.

frame travelling at the speed of the waves. However, the series of plots given in Figure 9 serve to illustrate the motion of the underlying flow structures for an Eulerian observer. The streamline plots illustrate qualitatively the countercurrent flow field produced by the moving, wavy surface. The plots indicate that the fluid under the wave crests travels at the speed of the waves. This flow is opposed by a countercurrent flow moving opposite the wave direction along the lower surface of the domain. Because of the height variation along the fluid domain, recirculation regions form between the opposing layers of fluid. These recirculating regions travel at the wave speed (when $c = U_S$) and are spatially periodic with the wave, although slightly offset from the wave crests. The flow structure is similar in character to that described by Sullivan *et al.* [9] in their computations of unconfined airflow over idealized waves. The plots of the horizontal velocity quantify the structure of the countercurrent flow over space and time. The structure is very similar to that generated by a flat moving surface except near the surface where the wave crests *trap* fluid and drag it along at the surface speed. This is made evident by the flatness of the velocity profiles beneath the wave crests. All of the velocity plots show virtually identical behaviour at the beginning and end of a spatial period, illustrating the periodicity of the flow and the accuracy of the periodic boundary conditions. The plots also implicitly illustrate that the solution is completely insensitive to the position of the periodic boundaries.

5. SUMMARY

A periodic boundary condition has been developed that can be used in conjunction with a specified flow rate to produce results in spatially periodic geometries. The flow rate is imposed at the inlet in terms of a bulk velocity, but the velocity profile evolves as part of the solution field. The periodic condition was shown to produce realistic results for flat and wavy-walled channels under both induced and countercurrent conditions. This condition is particularly useful in cases where the flow rate is known, or in cases where the pressure gradient across a spatial period is not known *a priori*, such as in countercurrent flows. While not shown in this paper, the periodic condition can be easily extended to three dimensions and include turbulence and scalar transport.

ACKNOWLEDGEMENTS

The author gratefully acknowledges financial support received from the Natural Sciences and Engineering Research Council of Canada.

REFERENCES

1. Sani RL, Gresho PM. Résumé and remarks on the open boundary condition minisymposium. *International Journal for Numerical Methods in Fluids* 1994; **18**:983–1008.
2. Nicolas X, Traore P, Majtabi A, Caltagirone JP. Augmented Lagrangian method and open boundary conditions in 2D simulation of Poiseuille–Benard channel flow. *International Journal for Numerical Methods in Fluids* 1997; **25**:265–283.
3. Orlanski I. A simple boundary condition for unbounded hyperbolic flows. *Journal of Computational Physics* 1976; **21**:251–269.
4. Patankar SV. *Numerical Heat Transfer and Fluid Flow*. Hemisphere: Washington, DC, 1980.
5. Ferziger JH, Perić M. *Computational Methods for Fluid Dynamics*. Springer: Berlin, 1996.

6. Rhie CM, Chow WL. Numerical study of the turbulent flow past an airfoil with trailing edge separation. *AIAA Journal* 1983; **2**:1527–1532.
7. Clift SS, D'Azevedo F, Forsyth PA, Knightly JR. *WATsitB sparse matrix solver*. The University of Waterloo: Waterloo, Canada.
8. Zhou H, Khayat R, Martinuzzi RJ, Straatman AG. On the validity of the perturbation approach for the flow inside a weakly modulated channel. *International Journal for Numerical Methods in Fluids* 2002; **39**:1139–1159.
9. Sullivan PP, McWilliams JC, Moeng CH. Simulation of turbulent flow over idealized waves. *Journal of Fluid Mechanics* 2000; **404**:47–85.

